PNAS RESEARCH ARTICLE | BIOPHYSICS AND COMPUTATIONAL BIOLOGY OPEN ACCESS

Affinity of disordered protein complexes is modulated by entropy–energy reinforcement

Milan Kumar Hazra[a] and Yaakov Levy[a,1]

Edited by Peter Wolynes, Rice University, Houston, TX; received November 9, 2021; accepted April 20, 2022

The association between two intrinsically disordered proteins (IDPs) may produce a fuzzy complex characterized by a high binding affinity, similar to that found in the ultrastable complexes formed between two well-structured proteins. Here, using coarse-grained simulations, we quantified the biophysical forces driving the formation of such fuzzy complexes. We found that the high-affinity complex formed between the highly and oppositely charged H1 and ProTα proteins is sensitive to electrostatic interactions. We investigated 52 variants of the complex by swapping charges between the two oppositely charged proteins to produce sequences whose negatively or positively charged residue content was more homogeneous or heterogenous (i.e., polyelectrolytic or polyampholytic, having higher or lower absolute net charges, respectively) than the wild type. We also changed the distributions of oppositely charged residues within each participating sequence to produce variants in which the charges were segregated or well mixed. Both types of changes significantly affect binding affinity in fuzzy complexes, which is governed by both enthalpy and entropy. The formation of H1–ProTa is supported by an increase in configurational entropy and by entropy due to counterion release. The latter can be twice as large as the former, illustrating the dominance of counterion entropy in modulating the binding thermodynamics. Complexes formed between proteins with greater absolute net charges are more stable, both enthalpically and entropically, indicating that enthalpy and entropy have a mutually reinforcing effect. The sensitivity of the thermodynamics of the complex to net charge and the charge pattern within each of the binding constituents may provide a means to achieve binding specificity between IDPs.

protein association | high-affinity binding | counterion entropy | intrinsically disordered proteins | polyelectrolytes

Significance

Intrinsically disordered proteins (IDPs), which are very common and essential to many biological activities, sometimes function via interaction with another IDP and form a fuzzy complex, which can be highly stable. It is unclear what the biophysical forces are that govern their thermodynamics and specificity, which are essential for *de novo* fuzzy complex design. Here, we explored the fuzzy complex formed between ProTα and H1, which are oppositely charged IDPs, by swapping the charges between them, generating variants that have either greater polyampholytic or polyelectrolytic nature as well as different charge patterns. Charge swapping and shuffling dramatically change the affinity of the fuzzy complex, which is contributed to by both enthalpy and entropy, where the latter is dominated by counterion release.

Protein–protein interactions are essential in molecular recognition (1–7) and, thus, essential to many biological functions. Chemical and structural complementarity are commonly found in many protein–protein recognition processes and determine their thermodynamic characteristics. The molecular details of the interface of the formed complex are often acknowledged to dictate its stability; nonetheless, it is not trivial to rationally design these properties via mutations. Although protein recognition between two folded proteins commonly occurs, intrinsically disordered proteins (IDPs) can also form complexes. IDPs may become more structured upon binding (8), but some remain unstructured and disordered even in the bound state and form "fuzzy" complexes (9–11) that rapidly interconvert between alternative states due to energetic frustration (12–14). The tendency of IDPs to interact with other IDPs is illustrated by their participation in various protein condensates formed by liquid–liquid phase separation, where IDPs largely retain their flexibility (15–21).

Similarly to the high affinity of some protein complexes formed by structured proteins, high affinity can also be found in binding between IDPs. Recently, ultrahigh-affinity binding was reported between human linker histone (H1) and nuclear protein prothymosin-α (ProTα), with both constituents remaining disordered in the H1–ProTα complex (22–24). The H1 protein is primarily involved in chromatin condensation, and the ProTα protein is involved in chromatin remodeling, cellular proliferation, apoptosis, and the transcription process. The functional advantage of such disorder in a complex is still the subject of debate; however, recent studies inferred that extreme disorder may considerably facilitate the regulatory mechanism (22, 23). Computational studies (25, 26) and single-molecule experiments (27) revealed that the presence of disorder in the positively charged H1 protein induces it to undergo large amplitude motions while on the nucleosome, with these facilitating its interaction with the negatively charged ProTα. As a result, ProTα can enter the H1–nucleosome complex and displace H1 by means of competitive substitution.

Consistently with the high and opposite absolute net charges on H1 (0.37 per residue, excluding the folded domain) and ProTα (−0.40 per residue), electrostatics was

Author affiliations: [a]Department of Chemical and Structural Biology, Weizmann Institute of Science, Rehovot 76100, Israel

Author contributions: M.K.H. and Y.L. designed research; M.K.H. performed research; M.K.H. and Y.L. analyzed data; and M.K.H. and Y.L. wrote the paper.

The authors declare no competing interest.

This article is a PNAS Direct Submission.

[1]To whom correspondence may be addressed. Email: koby.levy@weizmann.ac.il.

This article contains supporting information online at http://www.pnas.org/lookup/suppl/doi:10.1073/pnas.2120456119/-/DCSupplemental.

Published June 21, 2022.

found to play an important role in the formation of the fuzzy complex between them. Support for the role of electrostatics as a driving force is suggested by the strong effect of salt concentration on the dissociation constant (K_D) of the H1–ProTα complex. The high affinity of the fuzzy H1–ProTα complex (which is in the low picomolar range; ref. 23) is unique compared to the lower affinity measured for other fuzzy complexes (*SI Appendix*, Table S1 summarizes K_D of fuzzy complexes from the FuzDB database; ref. 28) and is quite unexpected, given its lack of shape and the absence of chemical complementarity, which are essential for the formation of high-affinity complexes between two well-folded proteins. Particularly high affinities involving structured proteins have been found for the *Escherichia Colicin* DNase–Im family of complexes formed between a bacterial toxin and its specific immunity protein, which exhibit K_D of 10^{-12} to 10^{-15} M (3, 5, 29). The barnase–barstar complex (which forms between an RNase and its inhibitor) is also characterized by very high affinity, with K_D of 10^{-13} M (at 300 K and a salt concentration of 300 mM) (30, 31).

The association of the highly charged disordered H1 and ProTα proteins is reminiscent of the condensates, particularly polyampholyte condensates, formed by some IDPs via liquid–liquid phase separation (16, 32–40). It was shown that long-range electrostatic interactions are essential to the stability of the condensate formed by charged IDPs and for maintenance of their internal mobility (41). Replacing long-range electrostatic interactions with short-range hydrophobic interactions affects the stability of the protein condensate (e.g., it lowers the critical temperature for phase separation) and its liquidlike properties (e.g., it lowers the intracondensate diffusion coefficient) (15). It was shown that changing the electrostatic properties of the IDPs by reorganizing the charges along their chains (i.e., by changing their charge pattern) also has a strong effect on stability and on the dynamics of the droplet (15, 41). These observations may suggest that the electrostatic properties of H1 and ProTα can dramatically affect the stability of their fuzzy complex.

Given that similarly high binding affinities have been found for the association of two IDPs and for two folded proteins, one may inquire whether both types of association reactions share similar thermodynamic driving forces. Similar thermodynamic properties were found for binding between two folded proteins and between a folded protein and an IDP (42). Often in these cases, binding reactions are dominated by a favorable change in enthalpy (ΔH) due to the formation of new interfacial interactions, with the change in entropy (ΔS) showing more complex behavior. Fuzzy complexes formed between two IDPs may make a larger entropic contribution to complex stability compared with binding between folded proteins or between a folded protein and an IDP. Moreover, it is unclear whether the entropy contribution can, in these cases, dominate the enthalpic contribution.

Furthermore, an unfavorable loss of entropy often compensates for the favorable enthalpic gain upon protein association, resulting in weaker stability. Although such enthalpy–entropy compensation may be sensitive to the ability to detect it experimentally (43), it is quite widespread and has been confirmed in various protein systems (44). The simplest physical explanation for the origin of enthalpy–entropy compensation is that the formation of favorable interfacial interactions in the bound state may be coupled with the imposition of conformational restrictions. Nonetheless, other molecular origins for enthalpy–entropy compensation may exist and may depend on the extent to which it occurs (44). Compensation between enthalpy and entropy is often probed in terms of similar ΔH and ΔS responses to modifications made to the two binding protein partners (namely, ΔΔH and ΔΔS share the same sign; therefore, the overall net effect on the free energy is small). For some systems, however, an opposite sign is measured for ΔΔH and ΔΔS that yields enhanced stability, suggesting the occurrence of enthalpy–entropy reinforcement (43, 45), although the microscopic interpretation of this phenomenon remains unclear. It is intriguing to ask whether the formation of fuzzy complexes exhibits enthalpy–entropy reinforcement or compensation.

The current study aimed to investigate the thermodynamic origin of the ultrahigh affinity of the fuzzy H1–ProTα complex and to quantify the cross-talks between enthalpy and entropy. We explored whether mutations affect the affinity of the fuzzy complex in a similar manner to the effect of mutations on the binding affinity of complexes between folded proteins. We applied coarse-grained (CG) molecular dynamics (MD) simulations to quantify the binding mechanism and thermodynamics of wild-type (WT) H1–ProTα as well as several of its mutants. As the complex involves highly charged proteins, we explored the effect on binding affinity of swapping charged residues between the two participating protein sequences (which affects their polyelectrolytic or polyampholytic character and, thus, their respective net charges) and within the sequences (which affects the charge pattern, i.e, the extent to which like charges are mixed or segregated within each sequence). We examined sets of variants of H1 and ProTα in an effort to comprehensively characterize the relationship between the various thermodynamic properties and the conformational ensemble of the complex.

Results and Discussion

Stability Analysis of Ordered and Disordered Protein Complexes. To study the mechanism and thermodynamics of the association of H1 and ProTα, extensive simulations of the CG model of their complex were performed to obtain their potential of mean force (PMF) profiles as a plot of their free energy (F) along the distance between their centers of mass (COMs) (R_{COM}). To obtain a better evaluation of the PMF of the high-affinity fuzzy complex formed by the H1 and ProTα IDPs, we also calculated the PMFs of the structured high-affinity complexes formed by the well-folded Im2 and Em2 proteins and by the barnase and barstar proteins (Fig. 1*A*). The PMF profiles of these three systems capture differences in the natures of the interactions within a fuzzy complex or an ordered-protein complex (Fig. 1*B* and *SI Appendix*, Fig. S1). The fuzzy complex H1–ProTα spans an almost 20-nm distance between the COMs of the two proteins (see *SI Appendix*, Fig. S2 for illustration of the long-range attraction between H1 and ProTα), whereas the PMF of the two ordered protein complexes is extremely sharp. This difference arises from fuzzy complex formation being driven by electrostatic interactions between highly charged proteins, whereas a folded protein complex characterized by relatively negligible charge content is stabilized by the formation of interfacial contact pairs between the two protein units. The electrostatic interactions are long range and persist as the proteins are drawn apart; however, the short-range contact pairs break down over much shorter distances.

To assess the predictive power of our model, we estimated the dissociation constants (K_D) of the three protein complexes. The deoxyribonuclease 2 and the immunity protein for colicin E2 (DNase2–Im2) and barnase–barstar complexes were chosen for reference, as they belong to a relatively well-studied, ordered protein complex family. The simulated K_D values were calculated as 4.3×10^{-10} M (at 200 mM NaCl) for H1–ProTα,

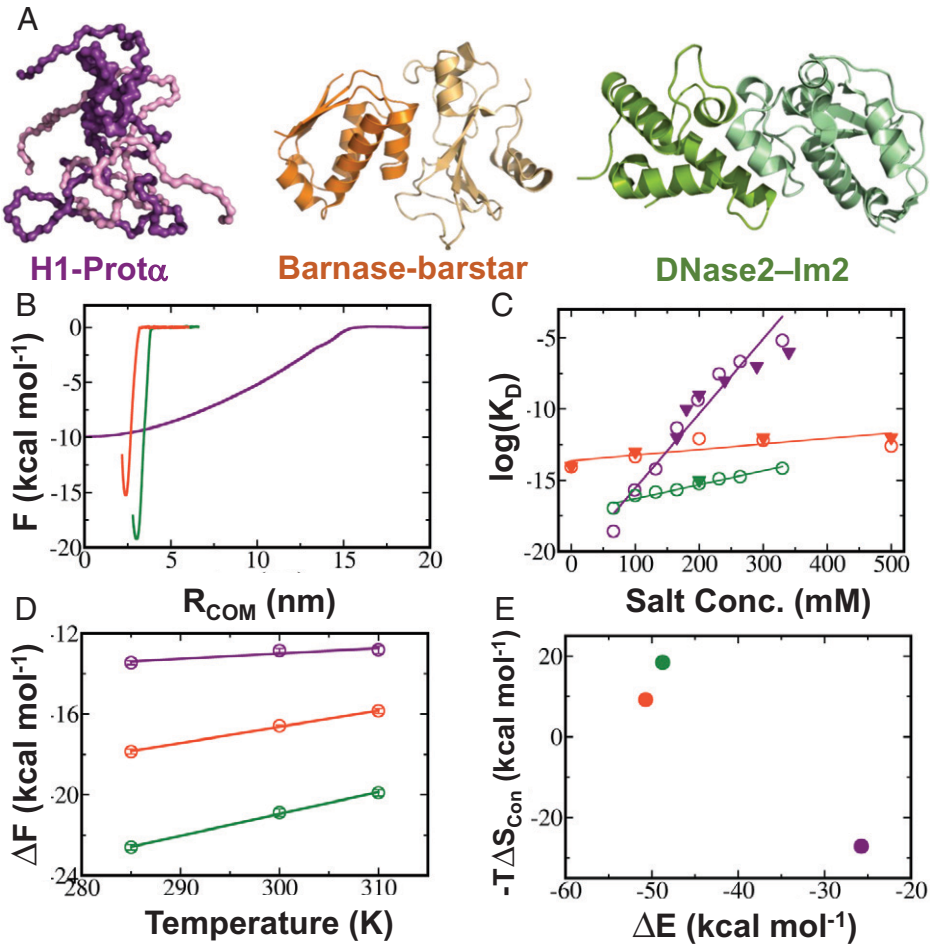

Fig. 1. Biophysical characterization of protein–protein binding between pairs of IDPs and pairs of structured proteins. (*A*) Structures of the H1–ProTα (purple) complex involving two IDPs and of the barnase–barstar (orange) and DNase2–Im2 (green) complexes involving structured (folded) proteins. The structures of barnase–barstar and DNase2–Im2 complexes were plotted using PDB ID 1BRS and 3U43, respectively. No structure is available for the ProTα–H1 complex because it is fuzzy; therefore, the presented snapshot is from MD simulations undertaken for this study. The folded domain of H1 was modeled using PDB ID 6N89. (*B*) PMF profiles of the H1–ProTα, barnase–barstar, and DNase2–Im2 complexes plotted as free energy (F) versus the distance between the centers of mass of the two interacting proteins (R_{COM}), shown using the same color code as that of their corresponding conformations in *A*. The PMFs were determined at a salt concertation of 200 mM and a temperature of 300 K. (*C*) Dependence of the dissociation coefficient, K_D, on salt concentration for the three complexes. The computationally estimated K_D values (empty circles fitted with a straight line) are shown together with the available experimental values (filled triangles). (*D*) Change in free energy for binding (ΔF) at three different temperatures for the three complexes. (*E*) Change in configurational entropy (represented here as $-T\Delta S_{Con}$) and enthalpy (ΔE) for the three complexes (obtained from simulating their bound and unbound states) at a temperature of 300 K and salt concentration of 200 mM (corresponding to Debye screening length of 0.9 nm).

6.41×10^{-13} M (at 300 mM NaCl) for barnase–barstar, and 5.5×10^{-16} M (at 200 mM NaCl) for DNase2–Im2 (Fig. 1*C*). In general, the simulated K_D values are consistent with the experimental K_D values, even at several salt concentrations. Fig. 1*C* shows that the experimental value of the salt-dependent K_D of H1–ProTα is in very good agreement with that simulated by our model. Similarly, for the DNase2–Im2 complex, at a salt concentration of 200 mM, we observe a strong match between the experimental and simulated K_D values ($\sim 10^{-15}$ M). The experimental dissociation constant data for the barnase–barstar complex (30, 31) also match the simulated K_D values at various salt concentrations in the 0- to 500-mM range. As expected, but unlike the H1–ProTα complex, the two complexes between structured proteins—namely, DNase2–Im2 and barnase–barstar—show a very weak dependence of stability on salt concentration because of the nature of the interaction involved (Fig. 1*C*).

The effect of temperature on stability (represented by ΔF; Fig. 1*D*) is somewhat opposite to the observed effect of salt on K_D (Fig. 1*C*). The total enthalpy and entropy can be obtained from the intercept and slope of the ΔF versus T curve, respectively. For the disordered H1–ProTα complex, $\Delta E^0 = -26.2$ kcal/mol and $\Delta S^0 = -0.02$ kcal/mol·K. The ordered DNase2–Im2 complex has lower values, with $\Delta E^0 = -53.6$ kcal/mol and $\Delta S^0 = -0.11$ kcal/mol·K, as does the ordered barnase–barstar complex, with $\Delta E^0 = -43.4$ kcal/mol and $\Delta S^0 = -0.09$ kcal/mol·K. These data imply that the entropy loss for the formation of an ordered protein complex is nearly four to five times larger than the entropy loss for the formation of a fuzzy protein complex. As temperature increases, the two structured protein complexes show a larger gradual destabilization, due to entropy loss, than that found for the fuzzy complex.

To understand the entropy better, we used the quasi-harmonic approximation, which uses covariance matrix obtained from three-dimensional Cartesian coordinates, to estimate the configurational entropy, S_{Con}, of the bound and unbound states of each of the three systems. We note that similar trends of configurational entropy were obtained by using the maximum information spanning tree (MIST) method (*SI Appendix*, Fig. S3).

Plotting $-T\Delta S_{Con}$ versus ΔE clearly highlights the difference between the association of two folded proteins and two IDPs. While both binding reactions are supported by a favorable enthalpic gain ($\Delta E < 0$), the configurational entropies have

opposite signs (Fig. 1*E*). The binding of two structured proteins is characterized by loss of configurational entropy ($-T\Delta S_{Con} > 0$); however, complex formation between two IDPs is accompanied by a configurational entropic gain ($-T\Delta S_{Con} < 0$). The free energy of the fuzzy H1–ProTα complex has almost no temperature dependence (Fig. 1*D*), which indicates that entropy may play a significant role in its stabilization. The fuzzy interactions in the H1–ProTα complex, thus, ensure an increase in configurational entropy; yet, this gain in configurational entropy is reduced by the loss of translational and rotational entropy (estimated to reduce binding free energy by about 10 to 15 kcal/mol; refs. 46, 47), as suggested by the nearly zero ΔS derived from Fig. 1*D*. In the next section, the configurational entropy and the potential contribution of the solvent entropy are further quantified.

Effect of Net Charge and Charge Pattern on the Stability of Fuzzy Complexes. H1 and ProTα are oppositely charged IDPs with total net charges of +45 and −44, respectively. These two IDPs, however, are not homogenously charged, with H1 containing four negatively charged residues and ProTα containing 10 positively charged residues. To understand the binding of H1 and ProTα better, we designed four additional variants of each IDP by swapping charges between them so that the net charge on each sequence varied while the net charge of their complex was held constant. In the designed variants, the net charge on H1 was +27 to +59, whereas that on ProTα was −26 to −58; however, the net charge of the complex was kept stable at +1. The five variants were designated variants A–E, where variant C was the WT. For H1, variant A had the lowest net charge, and variant E had the largest net charge, and similarly for ProTα (see Table 1). Variant E, with a net charge of +59 for H1 and −58 for ProTα, comprised two homogenously charged sequences (i.e., polyelectrolytes). Each of the five variants, A–E, of H1 and ProTα were further mutated by shuffling the charges within their sequences to modify the charge pattern without changing the respective charge contents. Sequence generation was guided by creating sequences with different degrees of segregation of the charged residues, as quantified by the κ measure (48). For each of the five variants of H1 and ProTα, three or four sequences were generated that covered a κ value range of 0.08 to 0.77 (see Table 1).

Following the mutation procedure, we generated 16 variants of H1 and 16 variants of ProTα, with both varying with respect to their net charge and their κ value. From these 32 variants, the association of 52 pairs of H1 and ProTα variants (nine pairs involving variants A, B, D, and E and 16 pairs involving variant C) were studied. We note that in all simulated H1 and ProTα pair associations, the total net charge of the complex equaled 1, consistently with the binding of WT proteins. Thus, we aimed to explore how the net charge on the constituent binding unit sequences of H1 and ProTα and their charge patterns affected the thermodynamics of their association.

The PMFs for binding of all the simulated pairs of the 34 designed variants A, C, and E are shown in Fig. 2*A* (in pink, purple, and blue, respectively). The PMFs illustrate that the association between H1 and ProTα is long range and starts to be attractive even when the distance between the COMs of the two proteins is greater than 20 nm. The PMFs are significantly affected by the net charge on the individual constituents of the complex, as illustrated by the clear clustering of the PMFs of all the sequences of variant A, whose PMFs are different from those of variants C or E. The charge pattern has a secondary nonnegligible effect on the PMF. The PMFs were integrated to estimate the K_D of the formed complex (see *Materials and Methods*).

Fig. 2*B* summarizes the K_D of the 52 simulated pairs of H1 and ProTα variants and pictorially illustrates how the K_D decreases when moving from variants A to E. The change in K_D for complexes of a given variant of H1 with different variants of ProTα (vertical lines) or of a given variant of ProTα with different variants of H1 (horizontal lines) is a manifestation of fuzziness for context-dependent binding. Fig. 2*C* further illustrates the strong effect that the net charge on the protein units has on the stability of their complex. Swapping about 20 charges between WT ProTα and H1 (i.e., variant C) results in sequences that are less homogenously charged (i.e., variant A), with K_D increasing by about 20 orders of magnitude and the overall stability of the fuzzy complex being low. In a similar manner, the K_D of the WT complex can be decreased. Swapping charged residues so that H1 and ProTα become more homogenously charged to create variant E results in extremely high-affinity binding, and K_D decreases by about 15 orders of magnitude. Modifying the charge pattern in the sequences of the five variant types of H1 and ProTα also affects K_D; however, its effect is weaker than that of the net charge. In Fig. 2*C*, the sequences are classified into three groups having low, medium, or high κ values (see *SI Appendix*, Fig. S4 for K_D vs. κ). For most variants, modifying κ changes K_D by about 10 orders of magnitude. It is evident, therefore, that the change in K_D strongly depends on both the net charge and the κ value.

Biophysical Driving Forces for the Formation of the Fuzzy Complex: Enthalpy versus Entropy. Understanding the relationship between affinity and the intrinsically disordered ProTα and H1 sequences required undertaking a detailed thermodynamic analysis. To quantify the role of the underlying thermodynamics in complex formation, we aimed to calculate the change in binding

Table 1. Designed sequence variants of H1 and ProT*α* with different charge content and charge pattern

Variant	H1 (119 residues)*			ProTα (110 residues)			
	Lys + Arg	Glu + Asp	Net charge	Lys + Arg	Glu + Asp	Net charge	Total net charge
A†	40	13	+27	19	45	−26	1
B†	44	9	+35	15	49	−34	1
C (WT)‡	49	4	+45	10	54	−44	1
D†	49	0	+49	10	−58	−48	1
E†	59	0	+59	0	−58	−58	1

*The values for H1 exclude the 74-residue folded domain in H1, which has 16 positively and 5 negatively charged residues.
†Three variants were designed for each of the H1 and ProTα proteins, with the sequences differing with respect to their charge pattern (as measured by the charge-patterning parameter, $0 < \kappa < 1$). From these sequences, all nine possible H1–ProTα complexes were simulated.
‡Four sequences were designed for each of the H1 and ProTα proteins, with the sequences differing with respect to their charge pattern (as measured by the charge-patterning parameter, $0 < \kappa < 1$). From these sequences, all 16 possible H1–ProTα complexes were simulated.

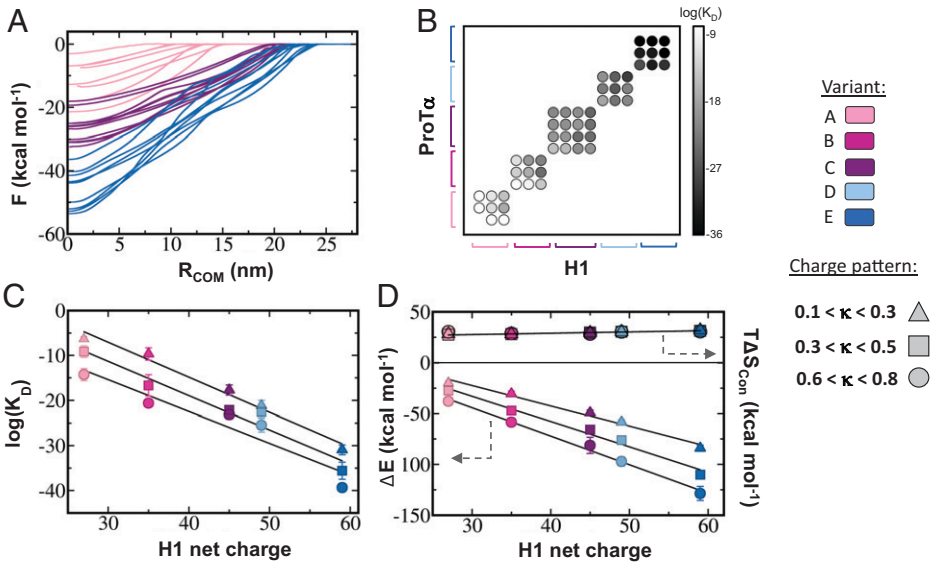

Fig. 2. Binding affinity of fuzzy complexes formed between variants of ProTα and H1. (*A*) PMF profiles for the binding of variants of ProTα and H1 that have different net charges plotted as a function of the distance between the centers of mass (R_{COM}) of the two constituent binding units. PMFs are shown for the association among variants A (low net charge, pink), C (medium net charge, purple), and E (high net charge, blue); see Table 1 for more details. For each of the variants, the PMF is simulated for ProTα and H1 having different patterning parameter, κ, values, where lower κ values indicate greater mixing of positively and negatively charged residues in the sequence, and higher κ values indicate greater segregation of charged residues into positively and negatively charged patches. It is evident that the PMF is affected by both the net charge and the charge pattern. (*B*) The dissociation constant (K_D) of the 52 simulated complexes of variants of H1–ProTα charge (see also Table 1). The sequences of variants A–E (marked by different colors) are ordered by their κ values (where the lowest κ value is on the left). (*C*) The K_D for binding between variants of ProTα and H1 plotted as a function of the net charge on H1 (note that for each variant, the net charge of the complex equals +1). The K_D of each variant A–E is colored according to its net. The K_D values of each variant are grouped based on their κ values: low κ (triangle), medium κ (square), and high κ (circle). The bars indicate SDs, which were calculated from all the sequences in each group. The K_D values for each H1–ProTα complex were measured at a salt concentration of 66 mM (corresponding to Debye screening length of 1.6 nm) and temperature of 300 K. A linear line is added for clarity to indicate the dependence of K_D on the net charge. (*D*) Enthalpy (ΔE; left *y* axis) and configurational entropy ($T\Delta S_{Con}$, right *y* axis) as a function of the net charge on H1 for the five H1–ProTα variants examined (variants A–E; see Table 1). A linear dependence of ΔE and $T\Delta S_{Con}$ on net charge is observed that is much stronger for the enthalpy than for the entropy. For higher net charge, a lower value is seen for ΔE and a greater value for TΔS, which indicates greater stability. The charge pattern (as represented by the charge-patterning parameter, κ) affects the value of ΔE of each type of variant: the higher the value of κ, the lower the value of ΔE (i.e., the greater the stability of the fuzzy complex) but has minor effect on the configurational entropy.

energy (ΔE) and in configurational entropy ($T\Delta S_{Con}$) upon complexation with respect to the isolated states for WT H1–ProTα and all its variants.

To understand the origin of the high affinity of fuzzy complexes, particularly its dependence on the net charge and charge pattern, we analyzed the changes in enthalpy (ΔE) and configurational entropy ($-T\Delta S_{Con}$) upon complex formation of the 52 studied complexes (Fig. 2*D*). In these and similar figures, the net charge on the H1 protein is represented by the color of the variant, with pink for a low net charge (more polyampholytic character) and blue for a high net charge (more homogeneously positively or negatively charged variants with a polyelectrolytic character). Charge pattern is represented by the symbol used for each datapoint, with triangles for variants with low κ values, squares for those with mid-κ values, and circles for those with high κ values. The overall charge of the bound complex was maintained at +1. Similarly, *SI Appendix*, Figs. S4 and S5 show E, ΔE, $-TS_{Con}$, and $-T\Delta S_{Con}$ plotted as a function of κ for all the variants. The values of ΔE become more negative as the absolute value of the net charge increases and the sequences become increasingly polyelectrolytic. This enthalpic gain from complexation increases about 3-fold from variants A to E (with a ΔΔE of about 100 kcal/mol) due to the change in the net charge on the two protein units. In particular, the binding of the homogenously charged variants of H1 and ProTα (variant E) is about 50% more energetically stable than the WT H1–ProTα complex (variant C). For each variant of ProTα and H1, varying the value of κ affects the ΔE of binding. The effect on ΔE of varying the κ values is smallest for variant A (ΔΔE ~ 25 kcal/mol as one moves between low and high κ values for ProTα and H1). A stronger effect of κ is observed for variant E (ΔΔE ~ 50 kcal/mol).

The dependence of ΔE on κ suggests that the inclusion of larger like-charged patches in the sequence (i.e., increasing κ) tends to stabilize the bound state. Such stabilization primarily originates from the bound state itself because of an enhancement of interactions among multiple patches (*SI Appendix*, Fig. S5). It is also important to note that the same effect stabilizes the unbound state for sequences with a lower net charge (i.e., for polyampholytic sequences), which diminishes energetic stabilization upon complexation for low net-charge systems as charge patterning (i.e., the value of κ) increases (*SI Appendix*, Figs. S5*C* and S6*A*).

The $-T\Delta S_{Con}$ term is also dependent on the net charge of H1 and ProTα (Figs. 2*D* *and* 3*A*); however, the overall effect is smaller than the effect of energy (Fig. 2*D*). The change in $-T\Delta S$ from variants A to E is about 4 kcal/mol. Changing κ has a weaker effect on $-T\Delta S$, but for some variants (e.g., C and E) the difference in configurational entropy between sequences of low and high κ can reach 1 kcal/mol. As κ increases in a sequence, we observe a slight rise in $-T\Delta S_{Con}$ for the sequences with high net charge (Fig. 2*D* and *SI Appendix*, Figs. S5 and S6), primarily due to the loss of degrees of freedom in the bound state itself. By contrast, sequences with low net charge show a decrease in $-T\Delta S_{Con}$ as a function of κ, due to a greater loss of conformational freedom in the unbound state than in the bound state as tighter interactions prevail in the unbound state of low net-charge sequences (i.e., those with

a greater polyampholytic character) (Fig. 2*D* and *SI Appendix*, Fig. S5).

To better understand the relationship between enthalpy and entropy, $-T\Delta S_{Con}$ was plotted against ΔE for low, intermediate, and high κ variants (Fig. 3*A* and *SI Appendix*, Fig. S6). It is interesting to note that $-T\Delta S_{Con}$ is negative for the formation of the fuzzy complexes formed between all the variants of H1 and ProTα, implying that configurational entropy stabilizes complex formation (Fig. 2*D*). Although biomolecular association is driven often by a favorable enthalpic change in the absence of any stabilizing entropic contribution (i.e., $\Delta H < 0$ and $-T\Delta S > 0$, as was found for barnase–barstar and DNase2–Im2; Fig. 1*E*), examples exist in which the association is driven by changes in both enthalpy and entropy (i.e., $\Delta H < 0$ and $-T\Delta S < 0$). We note that fuzzy complexes formed with IDPs may also be associated with entropic loss, given that they involve disorder-to-order transition (49). Association reactions involving a favorable entropic change can be found for protein–protein binding (both for folded proteins and IDPs; ref. 42) and for protein–ligand binding (50). In many of these cases, it is understood that the molecular origin of this favorable entropic contribution is linked to the release of solvent molecules upon binding as a result of the formation of contacts at the interface (51–55), rather than being linked to a favorable increase in configurational entropy, such as what we found for the fuzzy H1–ProTα complex.

One may observe that ΔE and $-T\Delta S_{Con}$ are correlated linearly to each other (Fig. 3*A*, solid black line), which implies a handshake between energy and entropy in stabilizing such a fuzzy complex, indicating the occurrence of enthalpy–entropy reinforcement rather than compensation. We note that enthalpy–entropy reinforcement is observed particularly upon changing the net charge of ProTα and H1 (i.e., from pink to blue across the different colored variants A–H). More complex behavior is seen when changing only κ (i.e., across the differently shaped datapoints). The three variant A sequences with different κ values, indeed, exhibit positive correlation between $-T\Delta S$ and ΔE; however, the three variant E sequences with different κ values exhibit anticorrelation between $-T\Delta S$ and ΔE, suggesting enthalpy–entropy compensation. As we move from systems with a high net charge (blue) to those with a low net charge (pink), the slope of the $-T\Delta S_{Con}$ versus ΔE curve shifts from negative to positive. Fig. 3*A* shows that for sequences with high net charge, as charge segregation (i.e., the value of κ) increases, energetic stabilization is coupled with entropic loss (i.e., enthalpy–entropy compensation occurs, which is dominated by the bound state; *SI Appendix*, Fig. S4). By contrast, for low net-charge sequences, as charge segregation increases, an entropic gain is accessed (i.e., enthalpy–entropy reinforcement occurs) along with energetic stabilization (which is dominated by the unbound state; *SI Appendix*, Fig. S5).

The favorable entropic contribution upon complexation is expected to be even larger upon accounting for entropy gain arising from the release of counterions, which is well acknowledged to govern polyelectrolyte complexation (56–59). This effect is not included in our model because of its high complexity but can be crudely estimated. To estimate the entropy of counterion release upon formation of H1–ProTα, we simulate all 52 variants of H1 and ProTα in the unbound state with counterions. In each case, the degree of counterion condensation, α, was measured from the simulations with explicit counterions to be between 0.09 and 0.18. This degree of counterion adsorption is consistent with the rough estimate that can be made based on the columbic strength parameter of H1 and ProTα if we treat them as polyelectrolytes. Given that their mean charge separation distances are 2 and 3, respectively, their

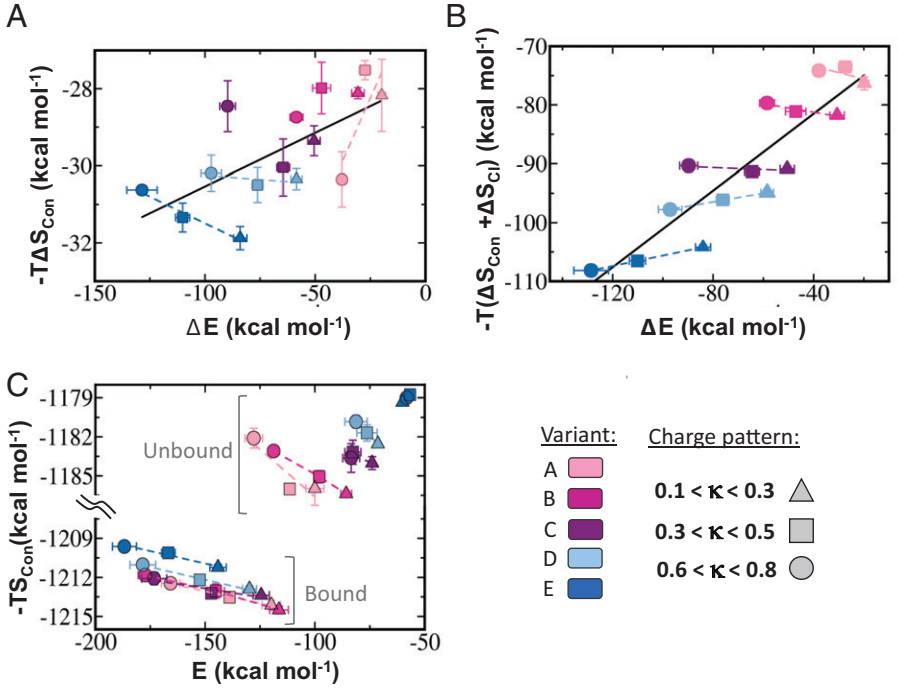

Fig. 3. Enthalpic and entropic analysis of the formation of fuzzy complexes. (*A*) Configuration entropy deference ($-T\Delta S_{Con}$) plotted against the ΔE between the bound and unbound isolated states for all the variants of the H1–ProTα system. A linear correlation (solid black line) is evident between $-T\Delta S_{Con}$ and ΔE, illustrating the occurrence of enthalpy–entropy reinforcement. Dashed lines are plotted for variants (namely, A, D, and E), demonstrating instances when modulating κ produces an enthalpy–entropy correlation in the opposite direction to that shown by the solid black line, consistently with the compensation mechanism. (*B*) Like *A*, with the exception that the contribution of the counterion's entropy is added to the configurational entropy. The counterion's entropy is estimated by calculating the degree of counterion's condensations to each variant of H1 and ProTα simulated in their unbound state with explicit counterions. (*C*) Plots of $-TS_{Con}$ versus E for bound proteins (*Lower Left*) and isolated unbound proteins (*Upper Right*) at a salt concentration of 66 mM at 300 K. Dashed lines are as for *C*. The bars indicate SDs, which were calculated from all the sequences in each group.

columbic strength parameters correspond to $\alpha \sim 0.1$ to 0.2 (we note that $\alpha \sim 0.5$ for fully charged polyelectrolytes; for the relationship between the columbic strength parameter and α, see Fig. 1 in ref. 60). For H1 and ProTα, a deviation from these values is expected, as these IDPs are not ideal (i.e., homogeneously charged) polyelectrolytes. Assuming that all counterions are released upon complexation, their entropic contribution from either H1 or ProTa is $\Delta S_{CI} \sim M n \Phi - N(1-\alpha)\ln[(1-\alpha)\Phi]$, where N is the number of counterions, and Φ is the volume fraction of the counterions. We found that the entropy from counterion release varies significantly between the variants, and it mostly depends on the net charge and less on κ. Variants with greater net charge or larger κ tend to adsorb more counterions, and, consequently, their complexes will have larger favorable entropy contributions from counterion release. The relationship between enthalpy and entropy when the counterion entropy is included (Fig. 3*B*) is similar to the case that includes the configurational entropy alone (Fig. 3*A*). The total entropy of counterions, $T\Delta S_{CI}$, at room temperature is between 40 and 80 kcal/mol, indicating that its contribution is more dominant than $T\Delta S_{Con}$. This highlights that the counterions may have a significant effect and that, overall, entropy may govern the stability of the fuzzy complex.

To understand the relative contributions of the bound and unbound states in energy–entropy reinforcement, we plotted $-TS_{Con}$ versus E for low, intermediate, and high κ values for all the variants (Fig. 3*C*; see also *SI Appendix*, Fig. S6). Fig. 3*C* shows that increasing the net charge on a sequence significantly increases $-T\Delta S_{Con}$. This increase can be observed for both the unbound states (*Upper Right*) and the bound states (*Lower Left*), with the unbound states exhibiting a much greater increase in $-T\Delta S_{Con}$ (i.e., a much larger decrease in the configuration entropy) as the net charge on a sequence increases.

Underlying Conformational Heterogeneity in Structure. As the thermodynamics of a complex is intimately connected to its structure, we examined the conformational space of the fuzzy complex formed between the different variants of H1 and ProTα. Fig. 4 shows the simulated bound state ensemble projected along the first two principal components (PCs) of the covariance matrix for complexes formed among sequences A, C, and E, for which the net charge on each sequences increasingly differs (see Table 1). The PC analysis (PCA) was performed for three different κ values (low, medium, and high κ shown in Fig. 4 *A*–*C*, respectively) for each variant. All variants of H1–ProTα exhibit a highly heterogeneous conformational ensemble because of the flexible nature of the two proteins in the complex. Increasing the net charge on the two sequences in the complex reduces the spread along the two principal coordinates, signifying a loss of conformational space. Consequently, configurational entropy decreases in the bound state as the net charge on the sequence increases (as is also shown in Fig. 3*D*, *Bottom Left*).

Charge pattern also affects the conformational heterogeneity of the formed complex. Fig. 4 shows that as κ increases, the configurational space of the bound state decreases (*SI Appendix*, Fig. S7). This indicates that both net charge and charge pattern affect the conformational dynamics of the complex.

We used a similar analysis to examine the dynamics of the unbound proteins. *SI Appendix*, Figs. S7 and S8 show PCAs for H1 and ProTα in the bound and isolated unbound states for several net-charge variants with low, intermediate, and high values of κ. It is interesting to note that charge pattern affects the configurational space in the unbound state of the two IDPs to a greater extent when their sequences have a polyampholytic character. As larger like-charged patches build up in a sequence with a low net charge, interactions between oppositely charged patches become strong enough to shrink the conformational space of the unbound state (*SI Appendix*, Figs. S8 and S9). Consequently, a larger entropy difference forms between the bound and unbound states for sequences with high κ values. As the net charge on the sequences increases, changing the charge pattern has no effect on the conformational dynamics in the unbound state, presumably because extensive repulsion between like charges dominates the flexibility of the sequences, regardless

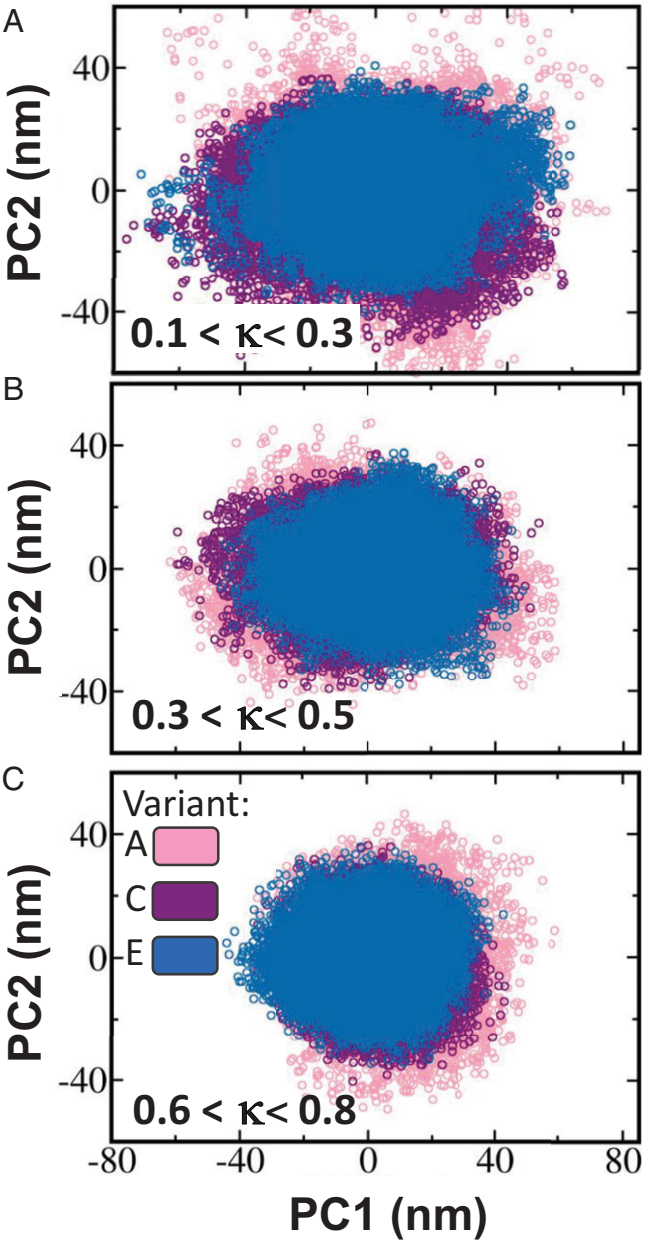

Fig. 4. Conformational space of the fuzzy complexes formed between variants of ProTα and H1. The simulated conformational ensembles of the bound complexes projected onto the first two PCs (PC1 and PC2) of the covariance matrix illustrate the conformational space of the bound state. The conformational analysis is shown for low net-charge variant A (pink), medium net-charge variant C (purple), and high net-charge variant E (blue) of H1 and ProTα (see Table 1 for more details). (*A*–*C*) Simultaneous projections for all three variants having (*A*) low, (*B*) intermediate, and (*C*) high charge-patterning (κ) values, as indicated on each panel. A heterogeneous conformational ensemble is observed for the fuzzy protein complexes, which reduces in size when the sequences have a higher net charge or larger κ values.

of their κ value. Unbound high net-charge sequences favor an elongated structure because of repulsion between like-charged residues, and, accordingly, charge pattern seems to have no effect on their conformational space (Fig. 3*C* and *SI Appendix*, Fig. S5*D*). However, the bound state of high net-charge sequences is further energetically stabilized as κ increases but has a reduced configurational space, resulting in affinity that is more dominated by enthalpy than by entropy (Fig. 3*C*).

We quantified the effect of net charge and charge distribution on the structure of the fuzzy complex formed between ProTα and H1 by probing the radius of gyration (Rg) of each protein. Fig. 5*A* shows the sum of the Rg values for the two proteins that form the disordered complex as a function of the net charge and for different κ values. Rg is markedly lower for the higher net-charge sequences, with their relatively higher polyelectrolyte character, implying a more collapsed and compact bound state for such sequences (Fig. 5*A* and *SI Appendix*, Fig. S10). Modulating the charge pattern also affects the Rg of the complex, such that within the same variant, Rg is smaller for proteins having larger κ. We observed that κ particularly affects the compactness of the complex for low net-charge proteins and has a milder effect on variants with high net charge. Representative snapshots capture the dependence on net charge and charge pattern of the bound-state structure for 9 out of the 52 studied variants (Fig. 5*B*). Compared with higher net-charge and higher κ variants, lower net-charge and lower κ variants exhibit a significantly more open structure in the bound state because their interaction sites are weaker.

Conclusions. The ability of some IDPs to form high-affinity fuzzy complexes is intriguing, given the lack of specific interactions and shape complementarity. Such high-affinity binding was measured recently for the H1–ProTα complex (23, 24). The K_D of such disordered complexes is similar to that measured for the most stable complexes formed between highly structured proteins (e.g., as found for the barnase–barstar and DNase2–Im2 complexes). However, it is unclear whether similar molecular driving forces control the formation of high-affinity protein complexes involving proteins with very different properties.

In this study, we used CG simulations to show that the fuzzy complex between H1 and ProTα is stabilized by favorable enthalpy, similarly to the structured barnase–barstar and DNase2–Im2 complexes. However, in contrast to the structured complexes, the fuzzy H1–ProTα complex is also stabilized by favorable entropy, which originates from the greater configurational entropy of its bound state compared to its unbound state. The increased configurational entropy in the bound state of the fuzzy complex is due to the relatively small entropy of the unbound state due to intrachain repulsion. In addition, due to the nonspecificity of the long-range electrostatics, significant exchange of interactions among many interacting oppositely charged patches may enhance the configurational entropy of bound state and contribute to its disordered nature. Such exchange of interactions is negligible in isolated proteins due to fewer oppositely charged motifs present. Although structured complexes are often destabilized entropically, entropic stabilization has been reported for some structured complexes, with such occurrences generally linked to the release of solvent upon complexation (53, 54), rather than to a change in the protein configurational entropy. The actual role of entropy in the stability of the fuzzy complex is expected to be further enhanced by the release of counterions attracted originally to the unbound highly charged proteins. Given the large counterion entropy, the overall entropic contribution to the complex thermodynamic stability may increase the enthalpic favorable contribution and, therefore, dominate the affinity of polyelectrolyte complexation. This effect might even be magnified by the expected less-favorable enthalpic contribution caused by screening

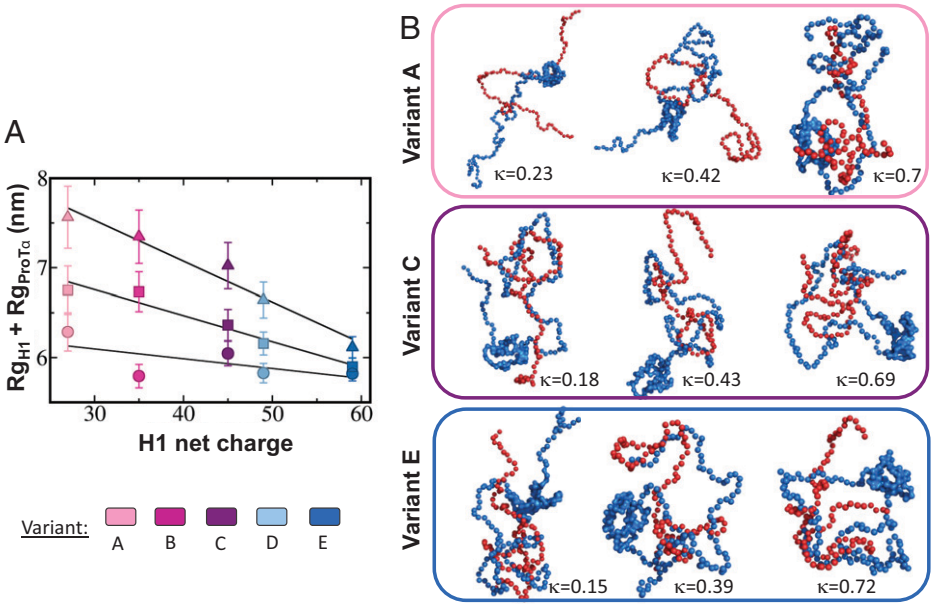

Fig. 5. Structural analysis of the fuzzy complexes formed between variants of ProTα and H1. (*A*) Sum of the Rg of ProTα and H1 in the bound state of their fuzzy complexes plotted against the net charge on H1 (corresponding to variants A–E; see Table 1 for more details). The different charge patterns on each of the simulated variants are grouped into three groups: low κ (triangle), medium κ (square), and high κ (circle). The bars indicate SDs, which were calculated from all the sequences in each group. Rg is linearly anticorrelated with the net charge, with the strongest anticorrelation for the sequences with lower κ values (i.e., the triangles). For the sequences with high κ, there is only a mild dependence of Rg on the net charge. (*B*) Representative snapshots of the bound complex formed among variants A, C, and E. Three sequences having low, medium, and high κ values are shown for complexes formed between pairs of each variant. The snapshots were selected to have Rg values close to the mean of the corresponding variant ensemble. In the snapshots, the H1 and ProTα sequences are shown in blue and red, respectively. The folded domain in H1 is shown as a surface. The exact κ value of the H1 and ProTα complex (being the average of the κ values of each of the two sequences) is indicated in each case.

by the adsorbed counterions in the unbound state. Nonetheless, counterion entropy may strongly depend on the net charge on each participating protein and on charge distribution, as these influence the tendency of the counterions to interact with charged polymers. This should be investigated in future studies.

We quantified the role of electrostatic forces in controlling binding affinity in fuzzy complexes by studying 52 complexes that encompassed a wide range of net charges and charge patterns in the participating sequences. We found that changing the net charge of each protein unit considerably affected binding affinity. The greater the difference in net charge between the two oppositely charged H1 and ProTα sequences, the greater their affinity. Manipulating κ by changing the distributions of oppositely charged residues along the linear sequence also affected binding affinity, with greater charge segregation (higher κ values) associated with greater binding affinity; however, the effect of charge pattern on binding affinity was more moderate compared with the effect of net charge. The sensitivity of the affinity of the fuzzy complex to the net charge on each sequence and to charge distribution, which can be interpreted in terms of energy frustration that has been recently linked to fuzziness (12), is reminiscent of their effect on the critical temperature and dynamics of IDP condensates formed via liquid–liquid phase separation (15, 41).

Binding between more homogeneously charged IDPs is characterized by a more negative ΔH, which is coupled with more negative −TΔS, indicating enthalpy–entropy reinforcement. Some cases of reinforcement between enthalpy and entropy have been reported (43, 45), yet their microscopic origin remained unclear. Recently, a favorable entropic contribution (i.e., $-T\Delta S < 0$) was measured for binding of small molecules to IDPs, illustrating the role entropy expansion may play for affinity and that IDP may increase their degree of disorder upon binding (61, 62). For the association of oppositely charged IDPs, the modulation of net charge shows that enthalpy–entropy reinforcement originates primarily from a change in the entropy of the unbound state. We note that changing the κ values of sequences with the same net charge may result in enthalpy–entropy compensation rather than reinforcement. This transition from enthalpy–entropy reinforcement to compensation demonstrates the high sensitivity of IDP complexation thermodynamics to the details of the sequence. Furthermore, the enthalpy–entropy relationship is also expected to be affected upon involvement of hydrophobic and pi-charge interactions, which are common in various IDPs and may change the thermodynamics of fuzzy complexes due to the change in the balance between long- and short-range interactions (15).

The binding of highly oppositely charged IDPs that remain disordered and dynamic in the bound state has been already observed for several systems (23, 63–66). The current study shows that notwithstanding the lack of structural complementarity and specificity, the polyelectrolytic properties of the IDPs as well as their charge patterns can bias the thermodynamics of the fuzzy complex. These features of the charged residues may serve to determine not only binding affinity, but also specificity.

Materials and Methods

Studied Systems. To understand how the net charge on a sequence and its charge pattern affect the stability of fuzzy protein complexes, we prepared five net-charge variants of the WT H1–ProTα complex by interchanging charged residues between the two oppositely charged proteins involved (Table 1). By swapping charges between H1 and ProTα, we designed sequences that had either greater polyelectrolytic character (i.e., they were more homogenously charged with either positively or negative residues and, thus, had a higher absolute net charge) or greater polyampholytic character (i.e., they contained a more even balance of positively and negatively charged residues and, thus, had a smaller absolute net charge). We then prepared 9 to 12 charge-pattern variants from each of the net-charge variants by scrambling the charged residues within the sequence. We used the patterning parameter (κ) to quantify the difference between various distributions of oppositely charged residues in a linear sequence, where $0 \le \kappa \le 1$ (48). In this manner, we obtained patterning parameter (κ) values ranging from nearly 0.10 (indicating strong mixing of charged residues within the linear sequence of each protein binding partner) to 0.8 (indicating strong segregation of oppositely charged residues within the linear sequence of each protein binding partner) (*SI Appendix*, Fig. S11).

Model. To analyze the stability of the disordered H1–ProTα complex and compare it with known ordered complexes, we applied a simple CG model for the proteins where each residue is represented as a single bead (67–70) and electrostatic interactions are applied between charged beads. The potential energy function consists of the following energies:

$$\begin{aligned} V = & \sum_{i<j\le N} \frac{1}{2} k^b_{ij}(d_{ij} - d^0_{ij})^2 + \sum_{i<j<k\le N-1} \frac{1}{2} k^a_{ijk}(\theta_{ijk} - \theta^0_{ijk})^2 \\ & + \sum_{i<j<k<l\le N-2} k^d_{ijkl}\left[\left(1 - \cos\left(\phi_{ijkl} - \phi^0_{ijkl}\right)\right) + 0.5\left(1 - \cos\left(3\left(\phi_{ijkl} - \phi^0_{ijkl}\right)\right)\right)\right] \\ & + K_{Coulomb} B(\kappa) \sum_{i,j} \frac{q_i q_j e^{-\kappa r_{ij}}}{\varepsilon r_{ij}} + \sum_{i,j\in native/interface} 4\varepsilon_c \left(\left(\frac{\sigma}{r_{ij}}\right)^{12} - \left(\frac{\sigma}{r_{ij}}\right)^{6}\right) \\ & + \sum_{i,j\in non-contacts} 4\varepsilon_{nc}\left(\left(\frac{\sigma}{r_{ij}}\right)^{12}\right) \end{aligned}$$

The first two terms represent bonded interactions and angular interactions with uniform force constants, with the third term representing dihedral angles. We used a dihedral force constant of 0.24 kcal/mol rad^2, which is low enough to capture the intrinsically disordered behavior of the H1–ProTα system. The next term defines the electrostatic contribution (6), where q_i and q_j represent the charge of the two amino acids involved in the interaction, r_{ij} is the interbead distance, ε is the dielectric constant of the solvent, and $K_{Coulomb} = 4\pi\varepsilon_0 = 332$ kcal/mol. The term $B(\kappa)$ is a function of salt concentration and the radius (a) of ions generated by the dissociation of the salt, and it is given by $B(\kappa) = \frac{e^{\kappa a}}{1+e^{\kappa a}}$. According to Debye-Hückel theory, the range of electrostatic interactions of an ion is of the order of κ^{-1}, which is called the Debye screening length. The Debye screening length is related to ionic strength as follows: $\kappa^2 = \frac{8\pi N_A e^2 \rho_A I}{1000\epsilon k_B T}$, where N_A is Avogadro's number, e is the charge of an electron, ρ_A is the solvent density, I denotes the ionic strength of the medium, k_B is the Boltzmann constant, and T denotes temperature.

In addition to the electrostatics, a short-range Lennard-Jones potential was used for the folded domains and for interface contacts in the ordered protein complexes. For the H1–ProTα system, this short-range interaction was applied only to the folded domain of histone and not to the interfaces. For the ordered protein complex DNase2–Im2, a uniform strength of $\varepsilon_C = 0.50$ kcal/mol was used for the interfacial pairs, but for folded domain pairs, the contact strength was set to $\varepsilon_C = 0.70$ kcal/mol. For the ordered barnase–barstar protein complex, a uniform strength of $\varepsilon_C = 0.55$ kcal/mol was used for the interfacial pairs, but for folded domain pairs, the contact strength was set to $\varepsilon_C = 0.70$ kcal/mol. GROMACS simulation package 5.1.5 (71) was used to run Langevin dynamics simulations with a friction coefficient of 0.1 ps^{-1} and a time step of 10 fs for a total of 2 μs for equilibration of the complexes.

Steered MD, umbrella sampling, and conformational entropy. The dissociation constants for the binding of the three selected systems (H1–ProTα, barnase–barnstar, and DNase2–Im2) were estimated from PMF profiles. The PMF was plotted as free energy (F) as a function of the distance between the COMs of the two interacting proteins (R_{COM}), with this distance used as the reaction coordinate. After the 2-μs equilibration, a pulling force was applied to the COM of ProTα at a pulling rate of 0.01 nm/ps and a pull force constant of 2.4 kcal/mol nm^2 to achieve a separation of 30 nm from the histone. Using steered MD to separate the two complexed proteins to a dissociation distance of 30 nm creates a vector between their COMs. The PMF was then estimated using the umbrella sampling technique by spacing 200 harmonic umbrellas at distances of 0 to 30 nm along the vector. Each

umbrella sampling window was equilibrated for 2 μs. The PMF profile was reconstructed from the equilibrated umbrella sampling windows using the weighted histogram analysis method (72). The convergence of the PMF profiles was confirmed for three selected systems (*SI Appendix*, Fig. S1).

The dissociation constant is related to the PMF by the following relation:

$$K_D = \frac{1}{4\pi N_{Av} \int_0^{R^b_{COM}} e^{-\beta F(R_{COM})} R^2_{COM} dR_{COM}};$$

where $\beta = \frac{1}{k_B T}$, and R^b_{COM} defines the maximum extent of the bound state. For the folded DNase2–Im2 and barnase–barstar protein complexes, steered MD was used to apply a force constant of 70 kcal/mol nm^2 with the same pull rate of 0.01 nm/ps to separate the two proteins to a dissociation distance of 10 nm. For the DNase2–Im2 and barnase–barstar complexes, 370 umbrella windows were spaced at a distance of 0 to 6 nm, while a pulling force constant of 200 kcal/mol nm^2 was applied to separate the COMs of each of the two protein units in the complex.

To determine the conformational entropy, we employed two methods that have been widely used in studies: quasi-harmonic analysis (73) and MIST (74), which produced very well-matched results. However, the MIST approach was found to be less sensitive to the κ parameter, most likely because obtaining the configurational entropy using the MIST approach involves a directly correlated movement of beads of up to a maximum of four atoms (a dihedral angle); however, charged patches demonstrate correlated movement over a longer range. The current paper discusses the results in light of the conformational entropy obtained from quasi-harmonic analysis, the details of which can be found in the *SI Appendix*.

Data Availability. All study data are included in the article and/or *SI Appendix*. All data discussed in the paper have been deposited in Open Science Framework (https://osf.io/4ysaz/) (75).

1. J. A. Wojdyla, S. J. Fleishman, D. Baker, C. Kleanthous, Structure of the ultra-high-affinity colicin E2 DNase–Im2 complex. *J. Mol. Biol.* **417**, 79–94 (2012).
2. A. H. Keeble, C. Kleanthous, The kinetic basis for dual recognition in colicin endonuclease-immunity protein complexes. *J. Mol. Biol.* **352**, 656–671 (2005).
3. N. A. Meenan *et al.*, The structural and energetic basis for high selectivity in a high-affinity protein-protein interaction. *Proc. Natl. Acad. Sci. U.S.A.* **107**, 10080–10085 (2010).
4. R. Wallis *et al.*, Protein-protein interactions in colicin E9 DNase-immunity protein complexes. 2. Cognate and noncognate interactions that span the millimolar to femtomolar affinity range. *Biochemistry* **34**, 13751–13759 (1995).
5. A. H. Keeble, N. Kirkpatrick, S. Shimizu, C. Kleanthous, Calorimetric dissection of colicin DNase–immunity protein complex specificity. *Biochemistry* **45**, 3243–3254 (2006).
6. R. Netzer *et al.*, Ultrahigh specificity in a network of computationally designed protein-interaction pairs. *Nat. Commun.* **9**, 5286 (2018).
7. K. B. Levin *et al.*, Following evolutionary paths to protein-protein interactions with high affinity and selectivity. *Nat. Struct. Mol. Biol.* **16**, 1049–1055 (2009).
8. P. E. Wright, H. J. Dyson, Intrinsically disordered proteins in cellular signalling and regulation. *Nat. Rev. Mol. Cell Biol.* **16**, 18–29 (2015).
9. M. Miskei *et al.*, Fuzziness enables context dependence of protein interactions. *FEBS Lett.* **591**, 2682–2695 (2017).
10. M. Fuxreiter, Fuzziness in protein interactions–A historical perspective. *J. Mol. Biol.* **430**, 2278–2287 (2018).
11. M. Fuxreiter, Classifying the binding modes of disordered proteins. *Int. J. Mol. Sci.* **21**, E8615 (2020).
12. S. Gianni *et al.*, Fuzziness and frustration in the energy landscape of protein folding, function, and assembly. *Acc. Chem. Res.* **54**, 1251–1259 (2021).
13. D. U. Ferreiro, E. A. Komives, P. G. Wolynes, Frustration in biomolecules. *Q. Rev. Biophys.* **47**, 285–363 (2014).
14. M. Chen *et al.*, Surveying biomolecular frustration at atomic resolution. *Nat. Commun.* **11**, 5944 (2020).
15. M. K. Hazra, Y. Levy, Biophysics of phase separation of disordered proteins is governed by balance between short- and long-range interactions. *J. Phys. Chem. B* **125**, 2202–2211 (2021).
16. A. Majumdar, P. Dogra, S. Maity, S. Mukhopadhyay, Liquid-liquid phase separation is driven by large-scale conformational unwinding and fluctuations of intrinsically disordered protein molecules. *J. Phys. Chem. Lett.* **10**, 3929–3936 (2019).
17. A. C. Murthy *et al.*, Molecular interactions underlying liquid-liquid phase separation of the FUS low-complexity domain. *Nat. Struct. Mol. Biol.* **26**, 637–648 (2019).
18. G. L. Dignon, W. Zheng, Y. C. Kim, R. B. Best, J. Mittal, Sequence determinants of protein phase behavior from a coarse-grained model. *PLOS Comput. Biol.* **14**, e1005941 (2018).
19. M. T. Wei *et al.*, Phase behaviour of disordered proteins underlying low density and high permeability of liquid organelles. *Nat. Chem.* **9**, 1118–1125 (2017).
20. C. W. Pak *et al.*, Sequence determinants of intracellular phase separation by complex coacervation of a disordered protein. *Mol. Cell* **63**, 72–85 (2016).
21. M. Vendruscolo, M. Fuxreiter, Sequence determinants of the aggregation of proteins within condensates generated by liquid-liquid phase separation. *J. Mol. Biol.* **434**, 167201 (2022).
22. A. Sottini *et al.*, Polyelectrolyte interactions enable rapid association and dissociation in high-affinity disordered protein complexes. *Nat. Commun.* **11**, 5736 (2020).
23. A. Borgia *et al.*, Extreme disorder in an ultrahigh-affinity protein complex. *Nature* **555**, 61–66 (2018).
24. B. Schuler *et al.*, Binding without folding–The biomolecular function of disordered polyelectrolyte complexes. *Curr. Opin. Struct. Biol.* **60**, 66–76 (2020).
25. H. Wu, P. G. Wolynes, G. A. Papoian, AWSEM-IDP: A coarse-grained force field for intrinsically disordered proteins. *J. Phys. Chem. B* **122**, 11115–11125 (2018).
26. H. Wu, Y. Dalal, G. A. Papoian, Binding dynamics of disordered linker histone H1 with a nucleosomal particle. *J. Mol. Biol.* **433**, 166881 (2021).
27. P. O. Heidarsson *et al.*, Release of linker histone from the nucleosome driven by polyelectrolyte competition with a disordered protein. *Nat. Chem.* **14**, 224–231 (2022).
28. A. Hatos, A. M. Monzon, S. C. E. Tosatto, D. Piovesan, M. Fuxreiter, FuzDB: A new phase in understanding fuzzy interactions. *Nucleic Acids Res.* **50** (D1), D509–D517 (2022).
29. W. Li, C. A. Dennis, G. R. Moore, R. James, C. Kleanthous, Protein-protein interaction specificity of Im9 for the endonuclease toxin colicin E9 defined by homologue-scanning mutagenesis. *J. Biol. Chem.* **272**, 22253–22258 (1997).
30. G. Schreiber, A. M. Buckle, A. R. Fersht, Stability and function: Two constraints in the evolution of barstar and other proteins. *Structure* **2**, 945–951 (1994).
31. G. Schreiber, A. R. Fersht, Interaction of barnase with its polypeptide inhibitor barstar studied by protein engineering. *Biochemistry* **32**, 5145–5150 (1993).
32. S. Elbaum-Garfinkle *et al.*, The disordered P granule protein LAF-1 drives phase separation into droplets with tunable viscosity and dynamics. *Proc. Natl. Acad. Sci. U.S.A.* **112**, 7189–7194 (2015).
33. A. S. Holehouse, R. V. Pappu, *Protein Polymers: Encoding Phase Transitions* (Nature Publishing Group, 2015), pp. 1083–1084.
34. C. P. Brangwynne, P. Tompa, R. V. Pappu, Polymer physics of intracellular phase transitions. *Nat. Phys.* **11**, 899–904 (2015).
35. J. McCarty, K. T. Delaney, S. P. O. Danielsen, G. H. Fredrickson, J. E. Shea, Complete phase diagram for liquid-liquid phase separation of intrinsically disordered proteins. *J. Phys. Chem. Lett.* **10**, 1644–1652 (2019).
36. A. Statt, H. Casademunt, C. P. Brangwynne, A. Z. Panagiotopoulos, Model for disordered proteins with strongly sequence-dependent liquid phase behavior. *J. Chem. Phys.* **152**, 075101–075101 (2020).
37. S. Das, A. N. Amin, Y. H. Lin, H. S. Chan, Coarse-grained residue-based models of disordered protein condensates: Utility and limitations of simple charge pattern parameters. *Phys. Chem. Chem. Phys.* **20**, 28558–28574 (2018).
38. J. P. Brady *et al.*, Structural and hydrodynamic properties of an intrinsically disordered region of a germ cell-specific protein on phase separation. *Proc. Natl. Acad. Sci. U.S.A.* **114**, E8194–E8203 (2017).
39. L. Sawle, K. Ghosh, A theoretical method to compute sequence dependent configurational properties in charged polymers and proteins. *J. Chem. Phys.* **143**, 085101 (2015).
40. J. Habchi, P. Tompa, S. Longhi, V. N. Uversky, Introducing protein intrinsic disorder. *Chem. Rev.* **114**, 6561–6588 (2014).
41. M. K. Hazra, Y. Levy, Charge pattern affects the structure and dynamics of polyampholyte condensates. *Phys. Chem. Chem. Phys.* **22**, 19368–19375 (2020).
42. K. Teilum, J. G. Olsen, B. B. Kragelund, Globular and disordered-the non-identical twins in protein-protein interactions. *Front. Mol. Biosci.* **2**, 40 (2015).
43. T. S. Olsson, J. E. Ladbury, W. R. Pitt, M. A. Williams, Extent of enthalpy-entropy compensation in protein-ligand interactions. *Protein Sci.* **20**, 1607–1618 (2011).
44. J. D. Chodera, D. L. Mobley, Entropy-enthalpy compensation: Role and ramifications in biomolecular ligand recognition and design. *Annu. Rev. Biophys.* **42**, 121–142 (2013).
45. E. Gallicchio, M. M. Kubo, R. M. Levy, Entropy-enthalpy compensation in solvation and ligand binding revisited. *J. Am. Chem. Soc.* **120**, 4526–4527 (1998).
46. M. I. Page, W. P. Jencks, Entropic contributions to rate accelerations in enzymic and intramolecular reactions and the chelate effect. *Proc. Natl. Acad. Sci. U.S.A.* **68**, 1678–1683 (1971).
47. C. W. Murray, M. L. Verdonk, The consequences of translational and rotational entropy lost by small molecules on binding to proteins. *J. Comput. Aided Mol. Des.* **16**, 741–753 (2002).
48. R. K. Das, R. V. Pappu, Conformations of intrinsically disordered proteins are influenced by linear sequence distributions of oppositely charged residues. *Proc. Natl. Acad. Sci. U.S.A.* **110**, 13392–13397 (2013).
49. S. Hadži, A. Mernik, Č. Podlipnik, R. Loris, J. Lah, The thermodynamic basis of the fuzzy interaction of an intrinsically disordered protein. *Angew. Chem. Int. Ed. Engl.* **56**, 14494–14497 (2017).
50. C. H. Reynolds, M. K. Holloway, Thermodynamics of ligand binding and efficiency. *ACS Med. Chem. Lett.* **2**, 433–437 (2011).
51. D. A. Renzoni *et al.*, Structural and thermodynamic characterization of the interaction of the SH3 domain from Fyn with the proline-rich binding site on the p85 subunit of PI3-kinase. *Biochemistry* **35**, 15646–15653 (1996).
52. M. Milos, J. J. Schaer, M. Comte, J. A. Cox, Microcalorimetric investigation of the interactions in the ternary complex calmodulin-calcium-melittin. *J. Biol. Chem.* **262**, 2746–2749 (1987).
53. G. J. Pielak, X. Wang, Interactions between yeast iso-1-cytochrome c and its peroxidase. *Biochemistry* **40**, 422–428 (2001).
54. R. D. Brokx, M. M. Lopez, H. J. Vogel, G. I. Makhatadze, Energetics of target peptide binding by calmodulin reveals different modes of binding. *J. Biol. Chem.* **276**, 14083–14091 (2001).
55. V. Mandiyan *et al.*, Thermodynamic studies of SHC phosphotyrosine interaction domain recognition of the NPXpY motif. *J. Biol. Chem.* **271**, 4770–4775 (1996).
56. A. V. Dobrynin, M. Rubinstein, Theory of polyelectrolytes in solutions and at surfaces. *Prog. Polym. Sci.* **30**, 1049–1118 (2005).
57. X. Xu, M. Kanduč, J. Wu, J. Dzubiella, Potential of mean force and transient states in polyelectrolyte pair complexation. *J. Chem. Phys.* **145**, 034901 (2016).
58. M. Muthukumar, Theory of counter-ion condensation on flexible polyelectrolytes: Adsorption mechanism. *J. Chem. Phys.* **120**, 9343–9350 (2004).
59. X. Xu *et al.*, Counterion-release entropy governs the inhibition of serum proteins by polyelectrolyte drugs. *Biomacromolecules* **19**, 409–416 (2018).
60. Z. Ou, M. Muthukumar, Entropy and enthalpy of polyelectrolyte complexation: Langevin dynamics simulations. *J. Chem. Phys.* **124**, 154902 (2006).
61. G. T. Heller, M. Bonomi, M. Vendruscolo, Structural ensemble modulation upon small-molecule binding to disordered proteins. *J. Mol. Biol.* **430**, 2288–2292 (2018).
62. G. T. Heller, P. Sormanni, M. Vendruscolo, Targeting disordered proteins with small molecules using entropy. *Trends Biochem. Sci.* **40**, 491–496 (2015).

63. E. D. Holmstrom, D. Nettels, B. Schuler, Conformational plasticity of Hepatitis C virus core protein enables RNA-induced formation of nucleocapsid-like particles. *J. Mol. Biol.* **430**, 2453–2467 (2018).
64. E. D. Holmstrom, Z. Liu, D. Nettels, R. B. Best, B. Schuler, Disordered RNA chaperones can enhance nucleic acid folding via local charge screening. *Nat. Commun.* **10**, 2453 (2019).
65. N. Danilenko *et al.*, Histone chaperone exploits intrinsic disorder to switch acetylation specificity. *Nat. Commun.* **10**, 3435 (2019).
66. A. L. Turner *et al.*, Highly disordered histone H1-DNA model complexes and their condensates. *Proc. Natl. Acad. Sci. U.S.A.* **115**, 11964–11969 (2018).
67. J. K. Noel *et al.*, SMOG 2: A versatile software package for generating structure-based models. *PLOS Comput. Biol.* **12**, e1004794 (2016).
68. J. K. Noel, P. C. Whitford, J. N. Onuchic, The shadow map: A general contact definition for capturing the dynamics of biomolecular folding and function. *J. Phys. Chem. B* **116**, 8692–8702 (2012).
69. P. C. Whitford *et al.*, An all-atom structure-based potential for proteins: Bridging minimal models with all-atom empirical forcefields. *Proteins* **75**, 430–441 (2009).
70. C. Clementi, H. Nymeyer, J. N. Onuchic, Topological and energetic factors: What determines the structural details of the transition state ensemble and "en-route" intermediates for protein folding? An investigation for small globular proteins. *J. Mol. Biol.* **298**, 937–953 (2000).
71. S. Pronk *et al.*, GROMACS 4.5: A high-throughput and highly parallel open source molecular simulation toolkit. *Bioinformatics* **29**, 845–854 (2013).
72. S. Kumar, J. M. Rosenberg, D. Bouzida, R. H. Swendsen, P. A. Kollman, The weighted histogram analysis method for free-energy calculations on biomolecules. I. The method. *J. Comput. Chem.* **13**, 1011–1021 (1992).
73. I. Andricioaei, M. Karplus, On the calculation of entropy from covariance matrices of the atomic fluctuations. *J. Chem. Phys.* **115**, 6289–6292 (2001).
74. M. Fleck, A. A. Polyansky, B. Zagrovic, PARENT: A parallel software suite for the calculation of configurational entropy in biomolecular systems. *J. Chem. Theory Comput.* **12**, 2055–2065 (2016).
75. M. K. Hazra, Y. Levy, Data_upload_pnas_hazra_levy_disordered_protein_complexes.tar.gz (Version: 1). Open Science Framework. https://osf.io/4ysaz/. Deposited 7 June 2022.